Supramolecular assembly of H-bonded copolymers/complexes/nanocomposites and fluorescence quenching effects of surface-modified gold nanoparticles on fluorescent copolymers containing pyridyl H-acceptors and acid H-donors†

Tzung-Chi Liang and Hong-Cheu Lin*

Received 6th January 2009, Accepted 20th April 2009
First published as an Advance Article on the web 22nd May 2009
DOI: 10.1039/b823450g

A series of photoluminescent (PL) and liquid crystalline (LC) self-H-bonded side-chain copolymers (**P1–P3**) consisting of pyridyl H-acceptors and isomeric acid H-donors (*i.e.*, *para*-, *meta*-, and *ortho*-benzoic acids) were synthesized. Supramolecular H-bonded complexes were also obtained by mixing the photoluminescent H-acceptor homopolymer **PBT1** (containing pyridyl pendants) with isomeric H-donor homopolymers **P7–P9**. The formation of H-bonds was confirmed by FTIR, DSC, and XRD measurements. Moreover, PL and LC properties of the H-bonded copolymers and complexes were affected not only by the H-bonding effect of the supramolecular structures but also by the acid-substituted positions of isomeric H-donors. In combination with different functionalized gold nanoparticles (which bear acid or acid-free surfactants), the emission intensities of nanocomposites containing self-H-bonded copolymer **P1** (bearing both H-acceptor and H-donor moieties) and non-self-H-bonded copolymer **P4** (bearing acid-protected moieties), were quenched to different extents by varying the concentration of gold nanoparticles. The copolymeric H-acceptors and surface-modified gold nanoparticles demonstrated diverse morphological and PL quenching effects on the supramolecular architectures of the nanocomposites, which result from competition between the H-donors from the acid pendants on copolymers and the acid surfactants on the gold nanoparticles.

Introduction

Self-assembled phenomena through molecular recognition between complementary constituents have been explored in various areas, such as biomaterials, liquid crystalline (LC) materials, and materials for electro-optical applications.[1–8] Not only can innovative LC properties of novel supramolecules consisting of two different components be generated through the intermolecular hetero-hydrogen-bonding interaction, but also the directed self-assembly of nano-scale building blocks using non-covalent interactions (*e.g.* hydrogen bonding, acid–base proton transfer, and electrostatic forces) has been amplified into macroscopically observable phenomena.[9] More recently, there has been considerable interest in conjugated polymers as highly sensitive chemosensors due to their potential applications in chemistry and biology.[10–15] This is based on the different fluorescence quenching capabilities caused by the varying degrees of supramolecular interactions with particular chemical or biological systems.[16–18] Poly(*p*-phenylene)s, poly(*p*-phenylene ethynylene)s, poly(*p*-phenylene vinylene)s, polythiophenes, and polyfluorenes with receptor groups, such as crown ethers, pyridine derivatives, and ionic groups, in the side-chains or main-chains have been successfully used for sensing ions and biological species.[19–25] The design and synthesis of fluorescent side-chain conjugated polymers which supramolecularly assemble and are able to exhibit either chromogenic and/or fluorogenic responses due to non-covalent interactions have gained considerable attention recently.[26–32]

Self-assembly of nanoparticles into nanocomposites provides a direct pathway for incorporating the particles' unique physical properties into the functional materials.[33] Due to the stability and biocompatibility of gold, gold nanoparticles protected by a mixed monolayer provide highly attractive models for biological and fluorescent conjugated polymers.[34,35] Many high performance fluorescence assay methods have been developed by taking advantage of this superquenching ability of gold nanoparticles for optically sensing biologically important ions and molecules. Gold nanoparticles can be functionalized so as to become soluble in water as well as in organic solvents with readily variable monolayer structures. Rotello and co-workers reported the synthesis and self-assembly of gold nanoparticles with inherent optical properties.[36–43] Murray and co-workers have investigated the quenching of fluorophores that are attached to monolayer-protected gold nanoparticles, and also the electron transfer from exited fluorophores to gold nanoparticles.[44,45] Direct binding between a fluorophore and a metal surface often results in the quenching of the fluorophore's excited states. In this scenario, both energy transfer and electron transfer processes are considered to be the major deactivation pathways for excited fluoroprobes on a metal surface.[46] Furthermore, in

Department of Materials Science and Engineering, National Chiao Tung University, Hsinchu, Taiwan, ROC. E-mail: linhc@cc.nctu.edu.tw; Fax: +8863-5724727; Tel: +8863-5712121 ext.55305

† Electronic supplementary information (ESI) available: Synthesis and characterization of monomers, polymers, and surface-functionalized gold nanoparticles **AuSC10** and **AuSCOOH**. See DOI: 10.1039/b823450g

the presence of other metal ions, such as Cu^{2+}, Co^{2+}, Fe^{3+}, Ni^{2+}, Zn^{2+}, Pb^{2+} and Ag^{+}, the gold nanoparticles of the quenched nanocomposites (containing fluorophores) can be replaced with the metal ions to different extents due to the stronger re-coordination or re-complexation of the metal ions with fluorophores, and therefore recover the fluorescence of the chromophores to behave as chemosensors.[47a,b] In addition, the gold nanoparticles of the quenched nanocomposites can also be reacted with reduced glutathione in the presence of a glutathione reductase enzyme, and then recover the fluorescence of the chromophores to behave as biosensors.[47c] The sensor applications from this work can be further developed to detect metal ions and biomolecules based on the modulation of fluorescence quenching and recovery.

Previously, several series of H-bonded fluorescent complexes/dendrimers and side-chain supramolecular polymers consisting of pyridyl fluorophores (small molecular H-acceptors) and various non-luminescent acid H-donors (including small molecules, dendrimers, and side-chain polymers) have been generated through intermolecular H-bonded interactions.[48,49] The purpose of this study was to explore photoluminescent (PL) self-H-bonded copolymers (**P1–P3**), consisting of *para*-, *meta*-, and *ortho*-benzoic acids (**M1–M3**) and fluorescent pyridyl (**PBT**) units (with an expected molar ratio of 1 : 1), for their potential application as proton donors (H-donors) and acceptors (H-acceptors), repectively. In order to evaluate the proton donating (H-donor) capabilities of the benzoic acid moieties, acid-protected monomers **M4–M6** (containing *para*-, *meta*-, and *ortho*-benzoic acid methyl ester units) and its successive acid-protected (non-self-H-bonded) copolymers **P4–P6** were synthesized.

Subsequently, it is more interesting to develop a two-stage self-assembly process in which the recognition (or sensing) of different surface-functionalized gold nanoparticles (with acid and acid-free surfactants) is proceeded by light-emitting copolymers, *i.e.*, self-H-bonded copolymer **P1** (bearing both H-acceptor and H-donor moieties) and non-self-H-bonded copolymer **P4** (bearing acid-protected moieties), correspondingly. Hence, side-chain conjugated copolymers bearing fluorescent pyridyl H-acceptor pendants not only behave as highly selective chemosensors for carboxylic acid H-donors, but also exhibit distinct fluorescent quenching effects upon the addition of surface-functionalized gold nanoparticles (*i.e.*, **AuSCOOH** and **AuSC10**, which contain acid and acid-free surfactants, respectively). To our knowledge, this approach (as shown in the schematic illustration of Fig. 1) is the first exploration of the supramolecular assembly of nanocomposites *via* fluorescence quenching and TEM morphological analysis. The competition between H-donors from the acid surfactants on the gold nanoparticles and the acid pendent groups on the copolymers to form H-bonds with the pyridyl pendants (as H-acceptors) of the copolymers will be surveyed.

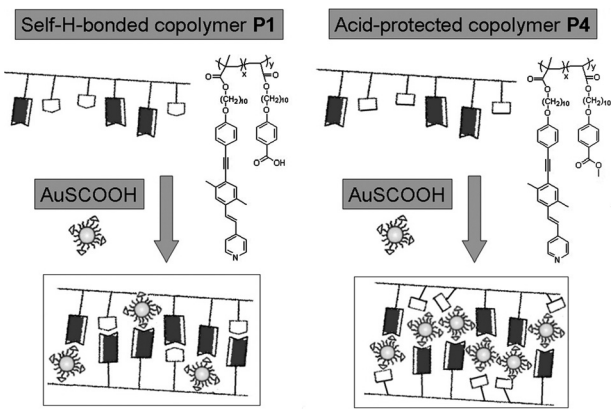

Fig. 1 Schematic illustration of acid-functionalized gold nanoparticles (**AuSCOOH**) blended with self-H-bonded copolymer **P1** and non-self-H-bonded copolymer **P4**.

Experimental section

Materials

Chemicals and solvents were reagent grade and purchased from Aldrich, ACROS, TCI, TEDIA, and Lancaster Chemical Co. Dichloromethane and THF were distilled before use. The other chemicals were used without further purification.

General synthetic procedures for monomers (M1–M6)

The synthetic route of the H-acceptor monomer **PBT** is described in the ESI† and isomeric H-donor monomers **M1–M3** (*i.e.*, *para*-, *meta*-, and *ortho*-benzoic acids) were prepared according to the procedure reported by Portugall *et al.*[50] Monomers **M4–M6**, with methyl-ester protecting groups, were also successfully synthesized by the same synthetic method as the H-donor monomers **M1–M3**. The chemical structures for all the products were confirmed by ^{1}H NMR spectroscopy and elemental analysis. The chemical characteristics of monomers **M1–M6**, *i.e.*, H-donor monomers (**M1–M3**) and acid-protected monomers (**M4–M6**), are outlined in the ESI.†

General synthetic procedures for copolymers (P1–P6)

According to Scheme 1, copolymers **P1–P6** were synthesized from monomers **M1–M6** (H-donor monomers **M1–M3** and acid-donor-protected monomers **M4–M6**) and the H-acceptor monomer **PBT**. Equal ratios of **PBT** (50%) and monomers **M1–M6** (50%), total amounts ~1.2 g, were dissolved in THF (6 mL) with AIBN (3 mol%) added as the initiator. The reaction mixture was flushed with nitrogen for 5 min, and then heated in a water bath at 60 °C to initiate polymerization. After 24 h, the reaction was terminated and the polymer was precipitated in a large amount of ether. The resulting copolymers **P1–P6** were re-dissolved several times in THF and re-precipitated in ether–hexane (1 : 1). The yields of the copolymers **P1–P6** were in the range 45–67%. The molecular weights and polydispersity index (PDI) values, relative to polystyrene standards, of copolymers **P1–P6** are presented in Table S1 (ESI†). The output compositions of copolymers **P1–P6**, *i.e.*, the molar ratios of monomer **PBT** to (H-donor or acid-protected) monomers **M1–M6**, which were estimated by NMR experiments, are also listed in Table S1. The ^{1}H NMR spectra of copolymers **P1–P6** are illustrated in Fig. S1 (ESI†). In the ^{1}H NMR spectra of copolymers **P1–P6**, the disappearance of proton peaks in the region of the vinyl units (chemical shifts at 5.4–6.1 ppm of methacrylate and acrylate groups) indicated that no monomers were present. The

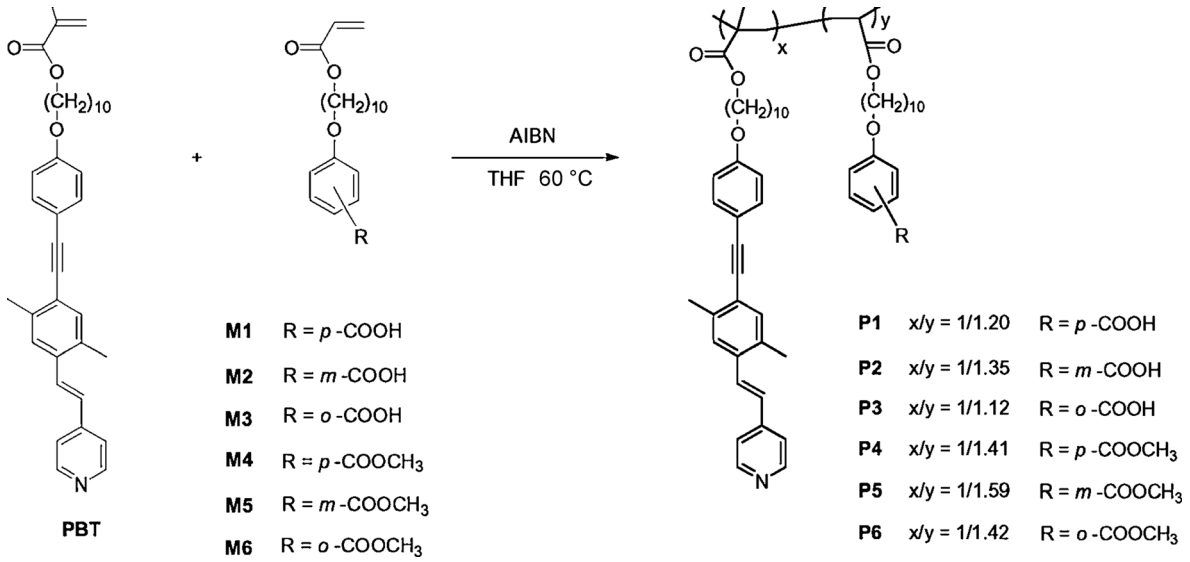

Scheme 1 Synthetic routes for copolymers **P1–P6**.

copolymer compositions in copolymers **P1–P6** were estimated by comparing the relative integration areas of the peak at 8.5 ppm, which belongs to the two protons of the α-pyridyl groups in **PBT**. The overlapped peaks from 6.7 to 7.9 ppm are assigned to the other aromatic proton regions in **PBT** groups as well as benzoic groups in **M1–M6**, respectively. The copolymer compositions (x/y = 1/y) were calculated by the following equation: x/y = 1/y = 1/[(total integration areas of aromatic protons in copolymer − total integration areas of aromatic protons in **PBT**)/(total integration areas of aromatic protons in **M1–M6**)] = 1/[(total integration areas of the aromatic protons in copolymer − 12)/4]. This is based on the assumption that the total integration area of the pyridyl protons nearest the heterocyclic N atom in each copolymer is equal to 2, *i.e.*, 2 protons. The chemical characteristics of polymers **P1–P6**, *i.e.*, H-donor polymers (**P1–P3**) and acid-protected polymers (**P4–P6**), are outlined in the ESI.†

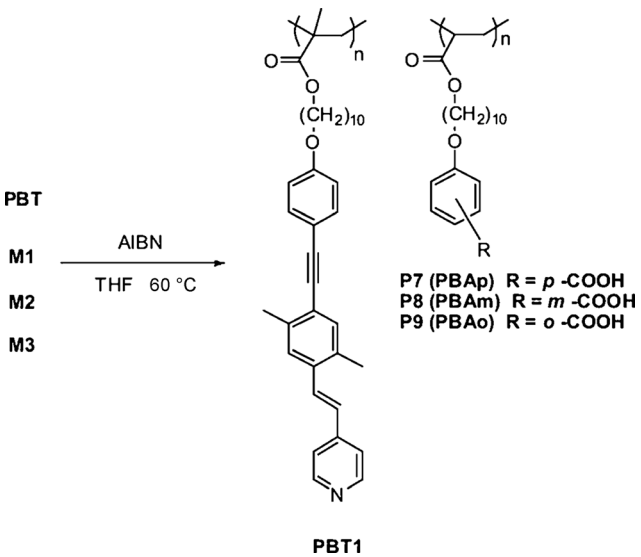

Scheme 2 Synthetic routes for H-acceptor homopolymer **PBT1** and H-donor homopolymers **P7–P9**.

Homopolymers PBT1 and P7–P9

By following Scheme 2, the H-acceptor monomer **PBT**, or H-donor monomers **M1–M3** (1 g) were dissolved in THF (5 mL) with AIBN (3 mol%) added as the initiator. The reaction mixture was flushed with nitrogen for 5 min and then heated in a water bath at 60 °C to initiate polymerization. After 24 h, the reaction was terminated and the polymer was precipitated into a large amount of ether. The homopolymers **PBT1** and **P7–P9** were re-dissolved in THF and re-precipitated in hexane several times. The yields were in the range 49–85%. The molecular weights and polydispersity index (PDI) values of homopolymers **PBT1** and **P7–P9** (*i.e.*, H-donor homopolymers **PBAp**, **PBAm**, and **PBAo**) are presented in Table S1 (ESI†).

Preparation of H-bonded complexes (PBT1/P7–P9)

All H-bonded complexes were fabricated from equal molar ratios of H-acceptor homopolymer **PBT1** and H-donor homopolymers **P7–P9** (**PBAp**, **PBAm**, and **PBAo**). The complexes were dissolved in THF to make a clear solution, and then subsequently dried for several hours in a vacuum oven at 60 °C. During solvent evaporation, the complexation through hydrogen bonding occurred between the H-donor and H-acceptor homopolymers. H-bonded complexes **PBT1/P7**, **PBT1/P8**, and **PBT1/P9**, which possess equal molar amounts of both pyridyl (H-acceptor) and carboxylic acid (H-donor) groups (1 : 1 molar ratio), were produced.

Preparation of nanocomposites consisting of gold nanoparticles and polymers

The surface-functionalized gold nanoparticles, **AuSCOOH** and **AuSC10**, which contain acid and acid-free surfactants, respectively, were synthesized according to the ESI.†Nanocomposites were prepared by mixing solutions (0.5 mg mL^{-1}) of surface-functionalized gold nanoparticles **AuSCOOH** and **AuSC10** in

THF. This was then mixed with solutions of copolymers **P1** and **P4** in DMF (2 mg mL^{-1}). The gold nanoparticles began to assemble into nanocomposites within 2 min. The mixed solutions became visibly turbid, indicating that an aggregation process had occurred. After 24 h, the solid precipitates were collected and washed extensively with hexane. The nanocomposites were then dried overnight before being subjected to transmission electron microscopy (TEM) measurements.

Characterizations

^{1}H NMR spectra were recorded on a Varian unity 300 MHz spectrometer using $CDCl_3$, DMSO-d_6, d-dioxane, and d-THF as solvents. Elemental analyses were performed on a HERAEUS CHN-OS RAPID elemental analyzer. Fourier transform infrared (FT-IR) spectra were performed on a Nicolet 360 FT-IR spectrometer. The textures of mesophases were characterized by a Leica DMLP polarizing optical microscope (POM) equipped with a hot stage (Linkam LTS350). Temperatures and enthalpies of phase transitions were determined by differential scanning calorimetry (DSC, model: Perkin Elmer Pyris 7) under N_2, at a heating and cooling rate of 10 °C min^{-1}. Thermogravimetric analyses (TGA) were conducted on a Du Pont Thermal Analyst 2100 system with a TGA 2950 thermogravimetric analyzer under N_2, at a heating rate of 20 °C min^{-1}. Molecular weights and molecular weight distributions were determined through gel permeation chromatography (GPC) using a Waters 510 HPLC, equipped with a 410 differential refractometer, a refractive index (RI) detector, and three Ultrastyragel columns (100, 500, and 103) connected in series in order to increase different pore sizes, with DMF as eluent at a flow rate of 0.6 mL min^{-1}. The molecular weight calibration curve was obtained using polystyrene standards. UV-visible absorption spectra in dilute THF solutions (10^{-6} M) were recorded on a HP G1103A spectrophotometer, and photoluminescence (PL) spectra in dilute THF solutions (10^{-6} M) were obtained on a Hitachi F-4500 spectrophotometer. Thin films for UV-vis and PL measurements were spin-coated (3000 rpm) on quartz substrates from THF solutions with a concentration of 1 wt%. The fluorescence quantum yields (Φ_{PL}) of the chromophores and H-bonded complexes were determined relative to a standard film of 9,10-diphenylanthracene dispersed in PMMA ($\Phi = 0.83$).[51] Synchrotron powder X-ray diffraction (XRD) measurements were performed at beamline BL17A1 of the National Synchrotron Radiation Research Center (NSRRC), Taiwan, where the X-ray wavelength was 1.32633 Å. The XRD data were collected using imaging plates (IP, of an area = 20 × 40 cm^2 and a pixel resolution of 100) curved with a radius equivalent to the sample-to-image plate distance of 280 mm, and the diffraction signals were accumulated for 3 min. The powder samples were packed into a capillary tube and heated by a heat gun, where the temperature controller was programmable by a PC with a PID feedback system. The scattering angle theta was calibrated by a mixture of silver behenate and silicon. Transmission electron microscopy (TEM) analyses were performed using a JEOL 2011 electron microscope with an acceleration voltage of 200 keV. The samples were prepared from THF solutions with a concentration of 1 wt%, and the aggregates were precipitated on TEM sample grids (200 Cu mesh–carbon films).

Results and discussion

Synthesis and characterization

Proton acceptor monomer **PBT** containing three-conjugated aromatic rings was successfully synthesized *via* Sonogashira coupling and Wittig–Horner reactions, whose synthetic route is illustrated in the ESI.†Two series of H-donor monomers **M1–M3** and acid-protected monomers **M4–M6** were synthesized. The molecular structures of monomers **M1–M6** were confirmed by ^{1}H NMR and elemental analysis. According to the synthetic routes shown in Scheme 1, copolymers **P1–P6** were synthesized from the H-acceptor monomer **PBT** along with monomers **M1–M6** (H-donor **M1–M3** and acid-protected **M4–M6**), with approximately 1 : 1 molar ratio, *via* the conventional synthesis of random free radical copolymerization. The random free radical polymerization of H-donor homopolymers **P7–P9** (**PBAp–PBAo**) and H-acceptor homopolymer **PBT1**, depicted in Scheme 2, were performed under the same conditions used in Scheme 1. The H-bonding effects on these two series of analogous copolymers, *i.e.*, self-H-bonded copolymers **P1–P3** and non-self-H-bonded copolymers **P4–P6** (containing H-donor monomers **M1–M3** and acid-protected monomers **M4–M6**, respectively), were evaluated for their thermal, mesogenic, and optical properties. The average molecular weights measured by gel permeation chromatography (GPC), relative to polystyrene standards, are displayed in Table S1 (ESI†). The number average molecular weights (M_n) of all polymers are between 5300 and 7100 g mol^{-1}, and the polydispersity index (PDI) values are between 1.4 and 2.6. Their thermal stabilities were measured under nitrogen by thermogravimetric analyses (TGA), and these results are also summarized in Table S1 (ESI†). The thermal decomposition temperatures (T_d) of 5% weight loss are between 284 and 389 °C, where the T_d values of polymers **P3** and **P9** exhibit the lowest thermal stability (284 and 294 °C, respectively) due to the isomeric effect from steric hindrance in the *ortho*-acid.

FT-IR spectroscopic studies

H-bonding effects in mesogenic copolymers **P1–P6** along with H-bonded complexes **PBT1/P7–P9** (H-acceptor homopolymer **PBT1** blended with H-donor homopolymers **P7–P9** in equal molar ratios) were confirmed by FT-IR spectroscopy. The IR spectra of the H-acceptor homopolymer **PBT1**, H-donor homopolymer **P7**, and their H-bonded complexes **PBT1/P7**, shown in Fig. 2(a), are compared in order to analyze the formation of H-bonds. In contrast to the O–H band of pure H-donor homopolymer **P7** (**PBAp**) at 2658 and 2543 cm^{-1}, the weaker O–H bands observed at 2528–2491 and 1931–1912 cm^{-1} in H-bonded complexes **PBT1/P7**, **PBT1/P8**, and **PBT1/P9** are indicative of stronger H-bonds formed between pyridyl groups of the H-acceptor homopolymer **PBT1** and acid groups of H-donor homopolymers **P7–P9** in their H-bonded complexes **PBT1/P7–P9**. On the other hand, a C=O stretching vibration appeared at 1730–1727 cm^{-1} in H-bonded complexes **PBT1/P7–P9** (a shoulder appeared at 1690 cm^{-1} for H-bonded complex **PBT1/P7**). This shows that the carbonyl group is in a more associated state than that it is in the pure H-donor homopolymer **P7**, which contains a weaker C=O stretching vibration at

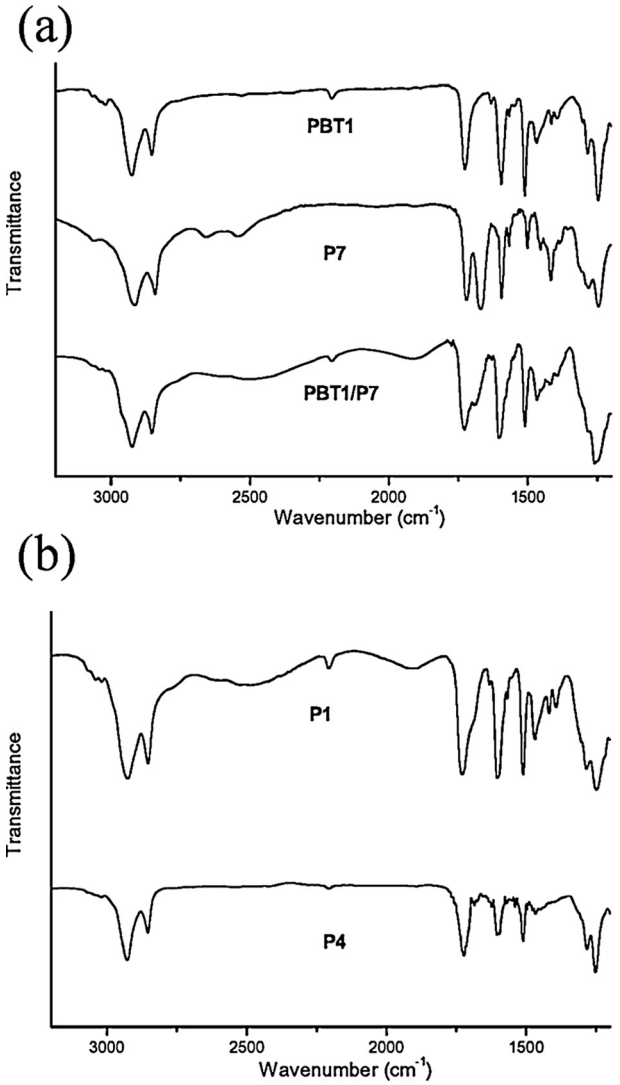

Fig. 2 Infrared spectra of (a) H-acceptor homopolymer **PBT1**, H-donor homopolymer **P7**, and H-bonded homopolymer complexes **PBT1/P7**; (b) copolymers **P1** and **P4** in solid films.

1720 and 1669 cm^{-1}. All results suggest that H-bonds were generated in the solid state of H-bonded complexes **PBT1/P7**, **PBT1/P8**, and **PBT1/P9**. As seen in Fig. 2(b), self-H-bonded copolymers **P1–P3** reveal similar IR spectral profiles to those [Fig. 2(a)]of H-bonded complexes **PBT1/P7–P9**, respectively. This suggests that analogous H-bonded structures formed in the self-H-bonded copolymers **P1–P3** and in the H-bonded complexes **PBT1/P7–P9**.[52] However, in comparison with self-H-bonded copolymers **P1**, acid-protected copolymer **P4** in Fig. 2(b) shows a weaker C=O stretching vibration at 1720 cm^{-1} because of the lack of a H-bonding interaction. The C=O stretching peak is sharper because there is less resonance for C=O stretching in the non-self-H-bonded copolymer **P4**, as well as acid-protected copolymers **P5–P6** because of a lack of H-bonds. Meanwhile, a shifted peak at 1600 cm^{-1} from a disturbance of the 1590 cm^{-1} ring mode, was observed in Fig. 2(a), which indicates a change in the strength of the acid–pyridine interactions.

Table 1 Thermal properties of polymers and H-bonded homopolymer complexes

Polymer/complex	Phase transition/°C[a]
PBT1[b]	Glass 51 N 145[c] I
P1	Glass 57 Sc 149 (3.7) I
P2	Glass 52 N 80[c] I
P3	Glass 42 N 69[c] I
P4	Glass 22 N 58[c] I
P5	Glass 22 N 47[c] I
P6	Glass 24 N 45[c] I
PBT1/P7[d]	Glass 53 Sc 167 (4.3) I
PBT1/P8[d]	Glass 30 N 94 (1.8) I
PBT1/P9[d]	Glass 24 N 80[c] I

[a] Phase transition temperatures (°C) and enthalpies (in parentheses, kJ mol^{-1}) were determined by DSC at a heating rate of 10 °C min^{-1}. [b] Phase transitions of **PBT** (monomer of homopolymer **PBT1**): K 42[c] N 71[c] I. [c] Phase transition temperatures were obtained by POM and confirmed by XRD. [d] No detectable T_g temperatures (by DSC) were observed in homopolymers **P7–P9**.

Phase characterization

The thermal properties (including glass transition temperatures (T_g) and isotropization temperatures (T_i) with corresponding enthalpies) of these copolymers and H-bonded complexes, determined by DSC and POM, are shown in Fig. S2 (ESI†) and Table 1. The glass transition temperatures of copolymers **P1–P6** and H-bonded complexes **PBT1/P7**, **PBT1/P8**, and **PBT1/P9** (H-acceptor homopolymer **PBT1** blended with H-donor homopolymers **P7–P9** in equal molar ratios) are *ca.* 22–57 °C. Moreover, all the self-H-bonded copolymers **P1–P3** containing H-donors have higher T_g and T_i values than their corresponding non-self-H-bonded copolymers **P4–P6**, which do not contain H-donors. This is because the self-H-bonded cross-linking polymer structures, in copolymers **P1–P3**, have a longer rigid core than the non-H-bonded side-chain polymer structures in acid-protected copolymers **P4–P6**. Both T_g and T_i values of H-bonded complexes **PBT1/P7**, **PBT1/P8**, and **PBT1/P9** show a similar trend (*i.e.*, **PBT1/P7 > PBT1/P8 > PBT1/P9**) as those of self-H-bonded copolymers **P1–P3** (*para*-acid-substituted copolymer **P1** > *meta*-acid-substituted copolymer **P2** > *ortho*-acid-substituted copolymer **P3**). Overall, the *para*-substituted copolymer **P1** and the H-bonded complex **PBT1/P7** exhibit the highest T_g and T_i values because they have the most linear H-bonded (cross-linked) structures.

Because of the linear H-bonded structures of self-H-bonded copolymer **P1** and H-bonded complex **PBT1/P7** (containing *para*-acid-substituted homopolymer **P7**), the smectic phase was only generated in the *para*-acid-substituted copolymer **P1** with a mesomorphic range of 92 °C and in the H-bonded complex **PBT1/P7** with a mesomorphic range of 114 °C. The H-bonded complex **PBT1/P7** had a wider mesophase range than the self-H-bonded copolymer **P1**, because the H-bonded complex (**PBT1/P7**) contains highly ordered H-bonded mesogens (from homopolymer blends) in the smectic arrangement. Due to the same reason of highly ordered H-bonds in H-bonded complexes, the nematic phases observed in nonlinear H-bonded structures (with non-*para*-acid-substituted H-donors) of H-bonded complexes **PBT1/P8** and **PBT1/P9** were wider than those of self-H-bonded copolymers **P2–P3**. This result suggests that the steric factor

related to the isomeric acid-substituted positions in H-donors is decisive for the formation of mesomorphism in all H-bonded structures. In addition, the acid-protected copolymers **P4–P6** (which lack H-bonds) possess the nematic phase adopted from the H-acceptor **PBT** moieties (with the nematic phase between 42 °C and 71 °C), which is similar to observations with the homopolymer **PBT1**. However, non-self-H-bonded copolymers **P4–P6** have lower phase transition temperatures (including the isotropization temperature T_i) than homopolymer **PBT1** due to the dilution effect of the acid-protected monomer moieties (**M4–M6**) in copolymers **P4–P6**.

To further elucidate the mesomorphic behavior in Table 1, POM and XRD measurements were performed at the mesophasic ranges of all copolymers and H-bonded complexes. The mesophases of copolymer **P1** and H-bonded complex **PBT1/P7** were characterized by POM. The textures of copolymers **P1** and **P2** identified by POM are shown in Fig. S3 (ESI†). To confirm the formation of the supramolecular structures, the smectic layer arrangements for copolymer **P1** and H-bonded complex **PBT1/P7** were characterized by *d*-spacing values of XRD measurements. The theoretical value of the fully-extended molecular length of copolymer **P1** is 57.8 Å, estimated using CS ChemOffice. The *d*-spacing values of copolymer **P1** and the H-bonded complex **PBT1/P7** at 130 °C are 50.3 and 52.4 Å, respectively [Fig. 3(a)]. These XRD measurements support the hypothesis that the copolymer **P1** and H-bonded complex **PBT1/P7** are suitable to be identified as the tilted smectic C phase with tilt angles of 29.6° and 25.0°, respectively. On the other hand, the absence of *d*-layer spacing peaks, for copolymers **P2–P6** and H-bonded complexes **PBT1/P8** and **PBT1/P9**, indicates that these species possess the nematic phase. For instance, Fig. 3(b) shows the XRD intensity against angle profiles obtained in the nematic phase of copolymer **P2** at 70 °C.

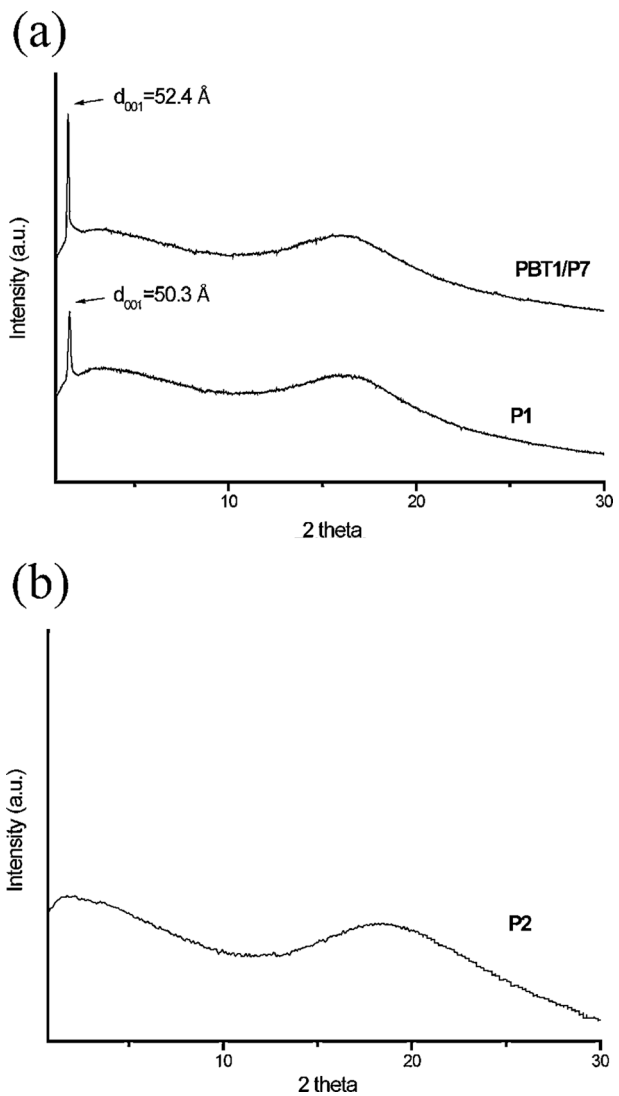

Fig. 3 (a) X-Ray diffraction (XRD) patterns of copolymer **P1** and H-bonded complex **PBT1/P7** in the Sc phase at 130 °C. (b) XRD intensity against angle profiles obtained in the nematic phase of copolymer **P2** at 70 °C.

Optical properties

The absorption and PL spectral data of all copolymers **P1–P6** (in both THF solutions and solid films) and H-bonded complexes **PBT1/P7**, **PBT1/P8**, and **PBT1/P9** (in solid films) are summarized in Table 2 and Fig. S4 (ESI†). As shown in Table 2, the maximum absorption peaks of copolymers **P1–P6**, near 350 nm (in THF solutions), are mainly attributed to the **PBT** units. In Table 2 and Fig. S4 (ESI†), PL emissions at 444–447 nm (in THF solutions) and at 515–529 nm (in solids for self-H-bonded copolymers **P1–P3**) are all red-shifted in contrast to PL emissions of acid-protected copolymers **P4–P6** (without H-bonds) at 429–431 nm (in THF solutions) and at 466–472 nm (in solids). Therefore, compared with PL emissions of non-self-H-bonded copolymers **P4–P6**, the H-bonding effects on PL emission wavelengths (λ_{max}) of self-H-bonded copolymers **P1–P3** are further enhanced in solids (red-shifted 43–63 nm) than in solutions (red-shifted 15–16 nm). However, due to the PL quenching effect by the aggregation of longer self-H-bonded chromophores in copolymers **P1–P3**, the acid-protected copolymers **P4–P6** (without H-bonds) exhibit higher PL quantum yields (in both solutions and solid films) than the self-H-bonded copolymers **P1–P3**. For all copolymers (**P1–P6**), it is apparent that more π–π stacking and molecular aggregation occur in solid films than in solutions. The aggregation phenomena are even more pronounced for **P1–P3** in solid films due to the self-H-bonded structures.

On the basis of our findings, non-luminescent acids are important for inducing various wavelength shifts in PL emissions of luminescent H-acceptors by tuning the pK_a values of H-donors in self-H-bonded copolymers and homopolymer complexes. The H-donor moieties with different pK_a values, *i.e.*, *para*-H-donor (**M1**): pK_a ~4.36; > *meta*-H-donor (**M2**): pK_a ~4.19; > *ortho*-H-donor (**M3**): pK_a ~4.15,[53] offer a solid solvent environment in the H-bonded copolymers and complexes. Therefore, the PL emission wavelengths of H-bonded complexes in solid films are related to the pK_a values as follows: **PBT1/P7** < **PBT1/P8** < **PBT1/P9**. Additionally, in contrast to self-H-bonded copolymers **P2** and **P3**, the *para*-substituted acid has the smallest acidity, and therefore the weakest H-donor effect which induces the smallest red-shifted PL emission in the solid film of copolymer **P1**. However, both acidic and steric effects of isomeric

Table 2 Absorption and PL emission spectral data of polymers and H-bonded homopolymer complexes in THF solutions and solid films

	Absorption λ_{max}/nm		PL emission λ_{max}/nm[b]			
Polymer/complex	Solution[a]	Film	Solution[a]	Film	Φ (%) (sol)[c]	Φ (%) (film)[d]
PBT1	350	357	440	487	40	20
P1	349	359	447	515	43	17
P2	349	361	445	529	39	14
P3	350	361	444	523	35	16
P4	347	359	431	472	58	22
P5	348	360	429	466	60	23
P6	349	360	429	466	60	26
PBT1/P7	—	358	—	514	—	18
PBT1/P8	—	363	—	522	—	16
PBT1/P9	—	360	—	525	—	15

[a] Absorption and PL emission spectra were recorded in dilute THF solutions at room temperature. [b] PL emissions were excited at the maximum absorption peaks. [c] PL quantum yield of 9,10-diphenylanthracene in THF (10^{-6} M) as the reference quantum yield in solution. [d] PL quantum yield of 9,10-diphenylanthracene blended in PMMA as the reference quantum yield in the solid film.

H-donors play important roles on the PL properties of H-bonded structures. The molecular π–π stacking in the H-bonded bending structures consisting of *meta*- and *ortho*-substituted H-donors were suppressed owing to the steric hindrance of *meta*- and *ortho*-substitution. Thus, the PL emission wavelengths of copolymers **P2** and **P3** in solid films have the following order: *meta*-**P2** (529 nm) > *ortho*-**P3** (523 nm), which is in the reverse order of acidity. In general, the results demonstrate that similar red-shifted PL emissions occur when isomeric H-donors are complexed to form supramolecular structures in both self-H-bonded copolymers (**P1–P3**) and H-bonded homopolymer complexes (**PBT1/P7–P9**). Moreover, the acidities and steric structures of the isomeric H-donors do affect the molecular packing and PL emission wavelengths of the H-bonded supramolecular architectures. Therefore, the λ_{max} values, which correspond to the emission colors, of the photoluminescence in the supramolecular systems can be tuned not only by adjusting the emitting cores but also by changing the isomeric structures of the H-donors.

Fluorescence quenching effects of copolymers by surface-modified gold nanoparticles

In the fluorescence quenching studies, where acid-donor-modified **AuSCOOH** nanoparticles and non-acid-modified **AuSC10** nanoparticles (diameter *ca.* 5–6 nm) were doped, the photoluminescence (PL) spectra of copolymers **P1** and **P4** were monitored in the presence of different concentrations of surface-modified gold nanoparticles (Fig. 4). The fluorescence spectra of pure copolymers **P1** and **P4** exhibit maximum PL emissions at 447 nm and 431 nm with corresponding quantum yields of 43% and 58%, respectively. In Fig. 4(a) and 4(b), copolymers **P1** and **P4** demonstrated dramatic decreases in fluorescence intensities upon the addition of **AuSCOOH** nanoparticles (which contain 21% carboxylic acid surfactants). Upon the addition of **AuSCOOH**, progressive fluorescence quenching effects on copolymer **P1** (blended with **AuSCOOH**) were observed by increasing the concentration of **AuSCOOH**. It is conceivable that the polymer nanocomposite **P1–AuSCOOH** reduced the fluorescence emission intensities by H-bonding complexation of the fluorescent pyridyl units with the acid surfactant on **AuSCOOH**. The H-donor (*para*-benzoic acid) units in the self-H-bonded copolymer **P1** were easily H-bonded with the pyridyl H-acceptor groups and competed with the acid H-donor surfactants on **AuSCOOH** nanoparticles. However, as shown in Fig. 4(b), the titration of acid-protected copolymer **P4** by **AuSCOOH** nanoparticles displays a similar PL quenching trend as Fig. 4(a). This suggests that the complexation of acid-protected copolymer **P4** and **AuSCOOH** nanoparticles has a similar H-bonding interaction as that in the nanocomposite **P1–AuSCOOH**. Unlike the self-H-bonded copolymer **P1**, there is no H-donor competition from the acid-protected copolymer **P4** during the H-bonding complexation process in the nanocomposite **P4–AuSCOOH**. Hence, the excitons of acid-protected copolymer **P4** are more easily trapped by the charge-transfer quenching of **AuSCOOH** than those of the self-H-bonded copolymer **P1**. As a comparison, the solutions of copolymers **P1** and **P4** were titrated with another nanoparticle counterpart, alkyl-functionalized gold nanoparticles (**AuSC10**, which bear acid-free surfactants). Both PL titrations of copolymers **P1** and **P4** by **AuSC10** nanoparticles [Fig. 4(c) and 4(d)]resulted in similar PL reductions after increasing the concentration of **AuSC10** nanoparticles. However, due to less H-bonding interactions of non-acid-modified **AuSC10** nanoparticles (containing acid-free surfactants) with copolymers **P1** and **P4**, **AuSC10** nanoparticles have much weaker PL quenching effects on **P1** and **P4** than acid-modified **AuSCOOH** nanoparticles [Fig. 4(a) and 4(b), respectively]. Comparing the insets of Fig. 4(a)–(d), the fluorescence quenching curves for copolymers **P1** and **P4** titrated by **AuSCOOH** [Fig. 4(a) and (b)] are totally different from those titrated by **AuSC10** [Fig. 4(c) and (d)]. The lower quenching effects observed for PL titrations of **AuSC10** nanoparticles on copolymers **P1** and **P4** are owed to the absence of H-bonding interactions between copolymers (**P1** and **P4**) and the acid-free surfactants on **AuSC10** nanoparticles.

The PL quenching behavior follows the Stern–Volmer relation $I_0/I = 1 + K_{SV}[Q]$,[54] where I_0 and I are the emission intensities of the fluorescent copolymers (**P1** and **P4**) in the absence and presence of the quencher Q (surface-modified gold nanoparticles), respectively, K_{SV} is the Stern–Volmer quenching constant, and [Q] is the concentration of the quencher. Fig. 5 demonstrates Stern–Volmer plots of copolymers **P1** and **P4** for various concentrations of acid-modified **AuSCOOH** nanoparticles and non-acid-modified **AuSC10** nanoparticles, which

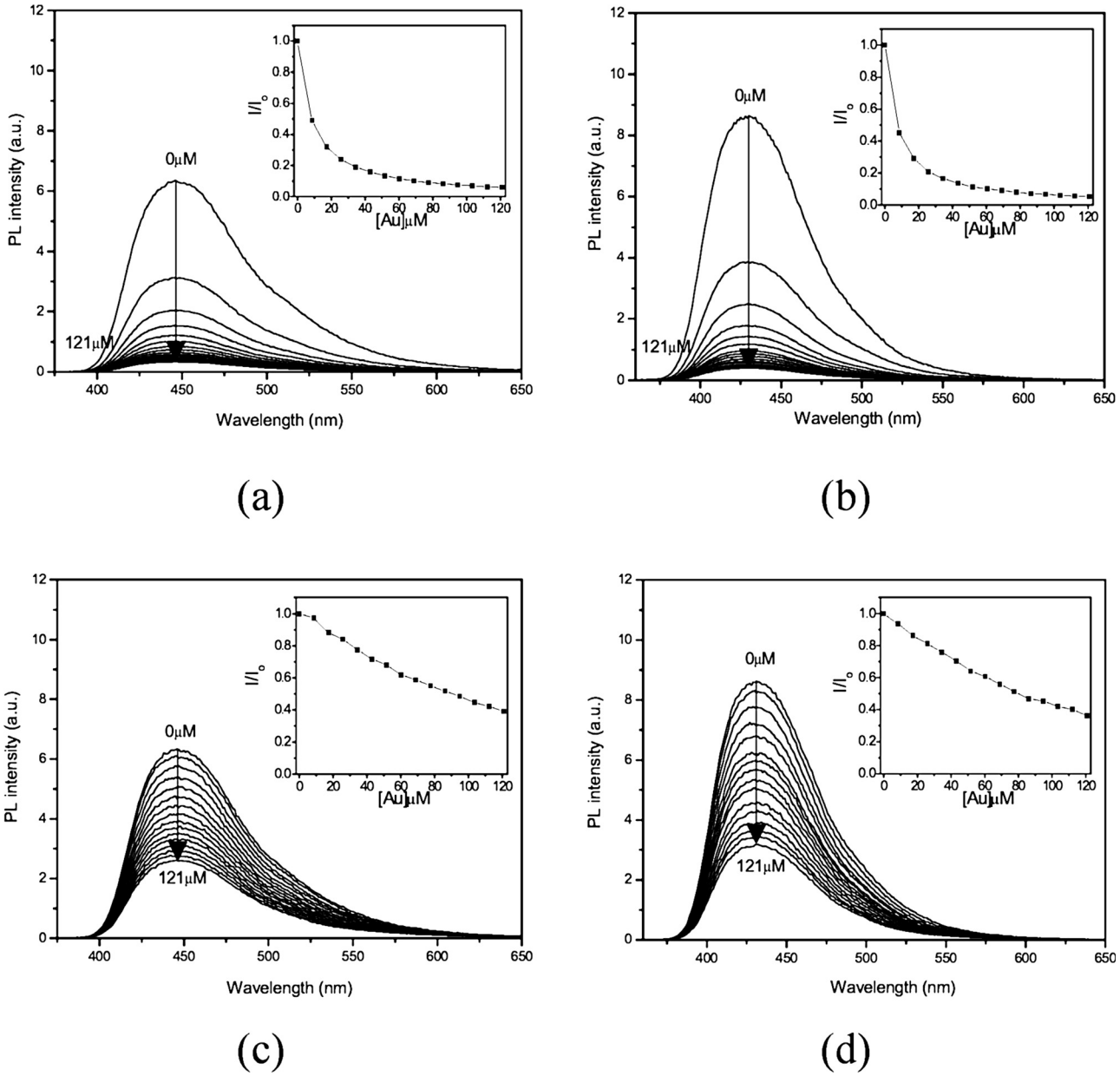

Fig. 4 Fluorescence quenching spectra of copolymers **P1** and **P4** titrated by surface-functionalized nanoparticles (**AuSCOOH** and **AuSC10**) in THF solutions: (a) **P1** and (b) **P4** by varying the concentration of acid-donor-modified gold nanoparticles (**AuSCOOH**); (c) **P1** and (d) **P4** by varying the concentration of non-acid-modified gold nanoparticles (**AuSC10**).

are replotted from the insets of Fig. 4(a)–(d). The quenching constants (K_{SV}) of copolymers **P1** and **P4** titrated with different nanoparticle quenchers (**AuSCOOH** and **AuSC10**) in THF solutions are obtained from the slope of Fig. 5 and listed in Table 3. In comparison with the fluorescence quenching effects of the **AuSCOOH** nanoparticles on copolymers **P1** and **P4**, the quenching constant ($K_{SV} = 1.20 \times 10^5\ M^{-1}$) of **P1** is smaller than that ($K_{SV} = 1.41 \times 10^5\ M^{-1}$) of **P4**. This can be explained by the partial self-quenching effect of H-bonds in copolymer **P1** (with a lower quantum yield than the non-self-H-bonded copolymer **P4**) which is induced by the higher aggregation of luminescent H-acceptor moieties in **P1** H-bonded to its own H-donor moieties. Similar to the previous results of copolymers **P1** and **P4** titrated with **AuSCOOH**, as copolymers were titrated with the **AuSC10** nanoparticles, the quenching constant ($K_{SV} = 1.32 \times 10^4\ M^{-1}$) of **P1** was slightly smaller ($K_{SV} = 1.57 \times 10^4\ M^{-1}$) than that of **P4**. Due to the reduced supramolecular interactions between **AuSC10** and copolymers **P1** and **P4** in the nanocomposites, both K_{SV} constants of copolymers **P1** and **P4** (1.32×10^4 and $1.57 \times 10^4\ M^{-1}$ without H-bonds) blended with non-acid-modified gold nanoparticles (**AuSC10**) are much smaller than those (1.20×10^5 and $1.41 \times 10^5\ M^{-1}$ with H-bonds) H-bonded with acid-donor-modified gold nanoparticles (**AuSCOOH**). Hence, the H-bonding interactions play an important role in our study of the fluorescence quenching effect. Moreover, it will be more interesting to develop a multicomponent self-assembly process

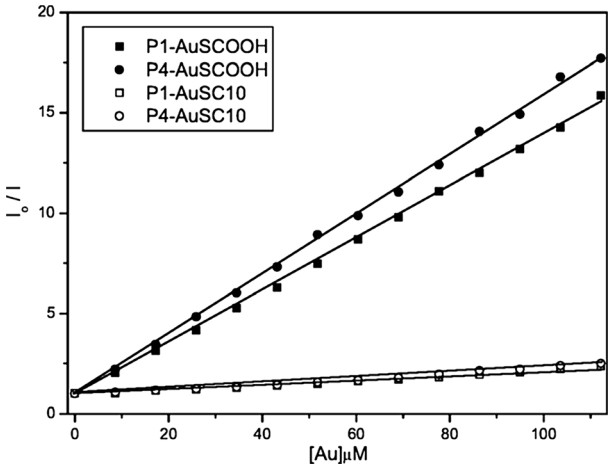

Fig. 5 Corresponding Stern–Volmer plots of copolymers **P1** and **P4** for increasing concentrations of acid-modified gold nanoparticles (**AuSCOOH**) and non-acid-modified gold nanoparticles (**AuSC10**) in THF solutions.

Table 3 Stern–Volmer constants (K_{SV}) of copolymers **P1** and **P4** titrated with different nanoparticle quenchers (**AuSCOOH** and **AuSC10**) in THF solutions

	K_{SV} (M^{-1})[a]	
	P1	**P4**
AuSCOOH	1.20×10^5	1.41×10^5
AuSC10	1.32×10^4	1.57×10^4

[a] The quenching behavior follows the Stern–Volmer relation $I_0/I = 1 + K_{SV}[Q]$, where I_0 and I are the emission intensities of the fluorescent copolymer (**P1** or **P4**) in the absence and presence of the quencher Q (surface-functionalized gold nanoparticles), respectively, K_{SV} is the Stern–Volmer quenching constant, and [Q] is the concentration of the quencher.

involving fluorescence quenching of pyridyl H-acceptors specifically by both acid H-donors from copolymer **P1** and acid-donor-modified gold nanoparticles (**AuSCOOH**). In general, the significant supramolecular interactions between various surface-modified gold nanoparticles and fluorescent polymers can be distinguished by the distinct fluorescence quenching behavior with specific quenching constants (K_{SV}). In order to confirm the fluorescence quenching effects on copolymers **P1** and **P4** by **AuSCOOH**, UV-visible absorption analyses of copolymer nanocomposites, containing **AuSCOOH**, were carried out. We would expect the UV-visible absorption spectra to change if the aggregation of fluorescent polymers is induced by the addition of **AuSCOOH**. In the UV-visible absorption spectra (Fig. S5, ESI†), the absorption peaks of copolymers **P1** and **P4** (350 and 520 nm in THF solutions) titrated by **AuSCOOH** do not red shift with increasing Au nanoparticle concentrations (from 0 to 121 μM). These were the same processing conditions used for the quenching titrations of fluorescent polymers **P1** and **P4** by Au nanoparticles. The reasonably low concentrations (smaller than 121 μM) of **AuSCOOH** were maintained to avoid the aggregation of fluorescent copolymers and **AuSCOOH** nanoparticles. Therefore, the aggregation effects on fluorescence quenching can be ignored. The major source of fluorescence quenching is then attributed to energy transfer between fluorescent copolymers (**P1** and **P4**) and Au nanoparticles (**AuSCOOH**).

TEM analysis

To further confirm the modulation of fluorescence quenching effects on copolymers **P1** and **P4** by acid-donor-modified gold nanoparticles (**AuSCOOH**), transmission electron microscopy (TEM) analysis was carried out on copolymer nanocomposites containing **AuSCOOH** nanoparticles. This provides a further insight into the morphology of the nanoparticle aggregation. Solutions of copolymer nanocomposites, consisting of **P1** and **P4** (2 mg mL^{-1}) blended with **AuSCOOH** (0.5 mg mL^{-1}) in THF solvent, were drop-cast onto TEM grids. The morphologies of the copolymer nanocomposites into structural ensembles were controlled by supramolecular self-assembly. Both carboxylic

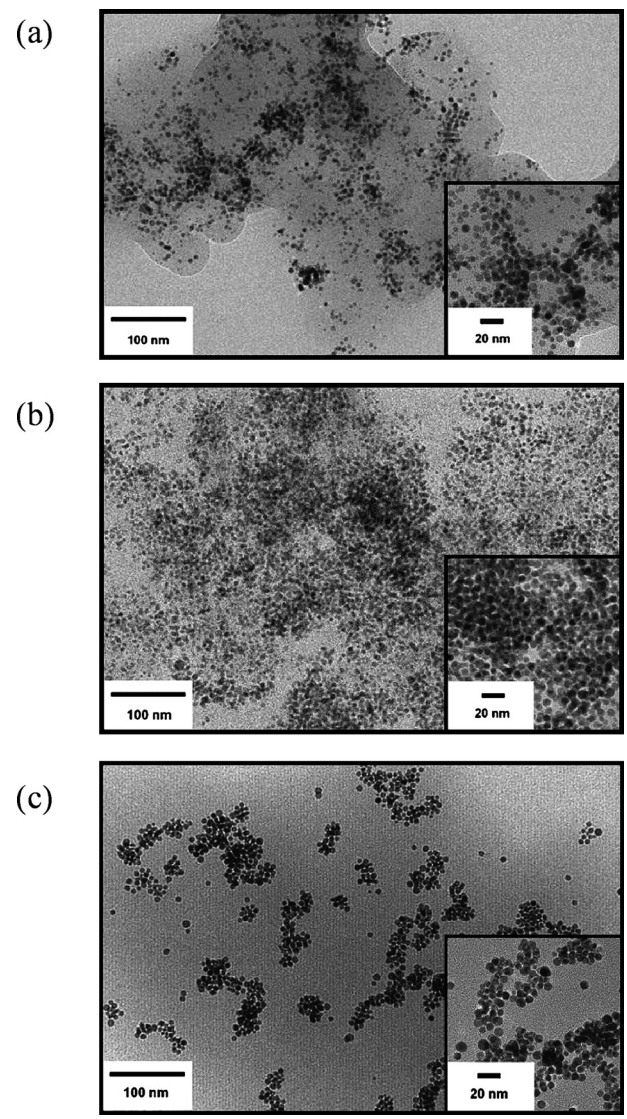

Fig. 6 TEM images of acid-functionalized gold nanoparticles (**AuSCOOH**) blended with (a) self-H-bonded copolymer **P1**, (b) acid-protected copolymer **P4**, and (c) alkyl-functionalized gold nanoparticles (**AuSC10**) blended with self-H-bonded copolymer **P1**.

acid units in surface-functionalized gold nanoparticles (**AuSCOOH**) and copolymer **P1** of nanocomposite **P1–AuSCOOH** will compete with each other to form H-bonds with the pyridyl groups on the copolymer **P1**. The addition of acid-modified gold nanoparticles (**AuSCOOH**) to copolymers **P1** and **P4** created two distinct aggregated structures. In Fig. 6(a), **AuSCOOH** nanoparticles (incompletely H-bonded to **P1**) were only partially dispersed in copolymer **P1**. This was due to the self-H-bonded copolymeric structures of the pendent pyridyl H-acceptors self-assembled with its own pendent H-donors in **P1**. Therefore, the layered self-H-bonded copolymeric structures of **P1** were clearly visible in this TEM micrograph. On the other hand, as **AuSCOOH** nanoparticles were blended with the non-self-H-bonded copolymer **P4**, more carboxylic acid surfactants from **AuSCOOH** nanoparticles were directly H-bonded with the pyridyl H-acceptor groups of the acid-protected copolymer **P4**. **AuSCOOH** nanoparticles were well distributed among copolymer **P4**, as shown in Fig. 6(b). The self-assembled phenomena of H-bonding between H-donors (from both copolymers and nanoparticles) and polymeric H-acceptors are dependent on all existing carboxylic acid groups (H-donors) available for the supramolecular architectures. Hence, **AuSCOOH** nanoparticles are more homogeneously dispersed in the acid-protected copolymer **P4** and less uniformly dispersed in self-H-bonded copolymer **P1**. Besides, as shown in Fig. S6 (ESI†), a similar aggregation trend of **AuSCOOH** nanoparticles was observed in the TEM images of nanocomposites containing various isomeric copolymers (self-H-bonded copolymers **P2** and **P3** and non-self-H-bonded copolymers **P5** and **P6**). In order to distinguish the contribution from the acid and acid-free surfactants on surface-modified nanoparticles (**AuSCOOH** and **AuSC10**, respectively), the self-H-bonded copolymer **P1** was blended with non-acid-modified **AuSC10** nanoparticles (without H-bonds between copolymer **P1** and **AuSC10** nanoparticles). Thus, it is clearly observed in Fig. 6(c) that non-acid-modified nanoparticles (**AuSC10**) aggregate more extensively. This suggests that no H-bonding interactions occurred between **AuSC10** nanoparticles and copolymer **P1**. Overall, the TEM morphologies of H-bonded architectures demonstrate the versatility of the self-assembly processes in supramolecular nanocomposites of H-acceptor polymers and H-donor nanoparticles.

Conclusions

In conclusion, the mesomorphic and photoluminescent properties of H-bonded copolymers and homopolymer complexes are affected by the isomeric H-donors with different acid-substituted (*para*, *meta*, and *ortho*) positions. These H-bonded complexes can generate supramolecular architectures either through self-H-bonded copolymers or by π-conjugated H-acceptor homopolymers blended with H-donor homopolymers. The supramolecular structures have the nematic and smectic C (Sc) phases that are related to their bent and linear H-bonded structures, respectively. The photoluminescent properties of self-H-bonded copolymers, as well as the H-bonded homopolymer complexes, can be tuned by the isomeric H-donor moieties, and red-shifted PL emissions are expected in the H-bonded structures. Supramolecular architectures that contain H-bonds in self-H-bonded copolymers **P1–P3** and H-bonded homopolymer complexes **PBT1/P7–P9** are further confirmed by FT-IR spectroscopy and XRD measurements. Furthermore, the H-bonding interactions between acid-modified gold nanoparticles (**AuSCOOH**) and acid-protected copolymer **P4** affect the fluorescence quenching more effectively, when compared with the fluorescence titrations of acid-free-modified gold nanoparticles (**AuSC10**). Moreover, in contrast to the self-H-bonded copolymer **P1**, the acid-protected copolymer **P4** more readily captures acid-modified gold nanoparticles (**AuSCOOH**) in the supramolecular assembly of nanocomposites. The H-bonding interactions between the pyridyl H-acceptor (from the copolymers) and the acid H-donor units (from both nanoparticles and copolymers) can explain the similarities in fluorescence quenching effects on both copolymers **P1** and **P4**. Various nanocomposites containing two kinds of fluorescent copolymer counterparts (self-H-bonded copolymer **P1** and acid-protected copolymer **P4**) and surface-modified nanoparticles (acid-modified **AuSCOOH** and acid-free-modified **AuSC10**) were developed to display distinct aggregation phenomena in TEM images. The pyridyl H-acceptor units of copolymer **P1** would not only bind with its own *para*-benzoic acid groups but also with the other proton donor surfactants from **AuSCOOH** nanoparticles. Overall, this study is the first to explore the supramolecular assembly behavior of nanocomposites between fluorescent copolymers and surface-functionalized gold nanoparticles *via* both PL quenching phenomena and TEM morphologies. Based on the fluorescence quenching and recovery of gold nanocomposites, further chemosensor and biosensor applications of this study can be developed in the near future.

Acknowledgements

We are grateful to the National Center for High-performance Computing for computer time and facilities. The powder XRD measurements are supported by beamline BL17A (charged by Dr Jey-Jau Lee) of the National Synchrotron Radiation Research Center (NSRRC), in Taiwan. The TEM measurements are supported by the Sinica, in Taiwan. The financial support provided by the National Science Council of Taiwan (ROC) through NSC 96-2113-M-009-015 and Chung-Shan Institute of Science and Technology (in Taiwan) are acknowledged for this project.

References

1 O. Ikkala and G. T. Brinke, *Science*, 2002, **295**, 2407.
2 S. I. Stupp, S. Son, H. C. Lin and L. S. Li, *Science*, 1993, **259**, 59.
3 T. Kato, N. Mizoshita and K. Kishimoto, *Angew. Chem., Int. Ed.*, 2006, **45**, 38.
4 (*a*) X. J. Ma, Y. T. Shen, K. Deng, H. Tang, S. B. Lei, C. Wang, Y. L. Yang and X. Z. Feng, *J. Mater. Chem.*, 2007, **17**, 4699; (*b*) X. J. Li, R. B. Wen, Y. Zhang, L. R. Zhu, B. L. Zhang and H. Q. Zhang, *J. Mater. Chem.*, 2009, **19**, 236; (*c*) T. Kajitani, S. Kohmoto, M. Yamamoto and K. Kishikawa, *J. Mater. Chem.*, 2004, **14**, 3449.
5 W. Pisula, Ž. Tomović, M. Wegner, R. Graf, M. J. Pouderoijen, E. W. Meijer and A. P. H. J. Schenning, *J. Mater. Chem.*, 2008, **18**, 2968.
6 Y. G. Liang, H. B. Wang, S. W. Yuan, Y. G. Lee, L. Gan and L. P. Yu, *J. Mater. Chem.*, 2007, **17**, 2183.
7 T. Kato, T. Matsuoka, M. Nishii, Y. Kamikawa, K. Kanie, T. Nishimura, E. Yashima and S. Ujiie, *Angew. Chem., Int. Ed.*, 2004, **43**, 1969.

8 H. Mamlouk, B. Heinrich, C. Bourgogne, B. Donnio, D. Guillon and D. Felder-Flesch, *J. Mater. Chem.*, 2007, **17**, 2199.
9 (*a*) M. Wanunu, R. P. Biro, H. Cohen, A. Vaskevich and I. Rubinstein, *J. Am. Chem. Soc.*, 2005, **127**, 9207; (*b*) S. O. Obare, R. E. Hollowell and C. J. Murphy, *Langmuir*, 2002, **18**, 10407.
10 T. M. Swager, *Acc. Chem. Res.*, 1998, **31**, 201.
11 L.-J. Fan and W. E. Jones Jr., *J. Am. Chem. Soc.*, 2006, **128**, 6784.
12 R. Martínez-Máñez and F. Sancenón, *Chem. Rev.*, 2003, **103**, 4419.
13 S. J. Broadwater, M. K. Hickey and D. T. McQuade, *J. Am. Chem. Soc.*, 2003, **125**, 11154.
14 L. J. Fan and W. E. Jones Jr., *J. Phys. Chem. B*, 2006, **110**, 7777.
15 A. Trabolsi, M. Elhabiri, M. Urbani, J. L. D. de la Cruz, F. Ajamaa, N. Solladié, A.-M. Albrecht-Gary and J. F. Nierengarten, *Chem. Commun.*, 2005, 5736.
16 S. W. Thomas III, G. D. Joly and T. M. Swager, *Chem. Rev.*, 2007, **107**, 1339.
17 (*a*) H. R. Li and S. Valiyaveettil, *Macromolecules*, 2007, **40**, 6057; (*b*) M. H. Nurmawati, P. K. Ajikumar, L. A. Heng, H. R. Li and S. Valiyaveettil, *Chem. Commun.*, 2008, 4945.
18 C. Tan, M. R. Pinto and K. S. Schanze, *Chem. Commun.*, 2002, 446.
19 B. S. Harrison, M. B. Ramey, J. R. Reynolds and K. S. Schanze, *J. Am. Chem. Soc.*, 2000, **122**, 8561.
20 W. H. Binder, R. Sachsenhofer, C. J. Straif and R. Zirbs, *J. Mater. Chem.*, 2007, **17**, 2125.
21 C. Fan, K. W. Plaxco and A. J. Heeger, *J. Am. Chem. Soc.*, 2002, **124**, 5642.
22 R. D. McCullough, P. C. Ewbank and R. S. Loewe, *J. Am. Chem. Soc.*, 1997, **119**, 633.
23 B. S. Gaylord, A. J. Heeger and G. C. Bazan, *J. Am. Chem. Soc.*, 2003, **125**, 896.
24 J. Kim, D. T. McQuade, S. K. McHugh and T. M. Swager, *Angew. Chem.*, 2000, **112**, 4026.
25 M. Kimura, T. Horai, K. Hanabusa and H. Shirai, *Adv. Mater.*, 1998, **10**, 459.
26 K. G. Thomas and P. V. Kamat, *Acc. Chem. Res.*, 2003, **36**, 888.
27 A. Bayir, B. J. Jordan, A. Verma, M. A. Pollier, G. Cooke and V. M. Rotello, *Chem. Commun.*, 2006, 4033.
28 S. Barazzouk, P. V. Kamat and S. Hotchandani, *J. Phys. Chem. B*, 2005, **109**, 716.
29 T. Hasobe, K. Saito, P. V. Kamat, V. Troiani, H. Qiu, N. Solladié, K. S. Kim, J. K. Park, D. Kim, F. D'Souza and S. Fukuzumi, *J. Mater. Chem.*, 2007, **17**, 4160.
30 B. Gadenne, I. Yildiz, M. Amelia, F. Ciesa, A. Secchi, A. Arduini, A. Credi and F. M. Raymo, *J. Mater. Chem.*, 2008, **18**, 2022.
31 A. C. W. Leung and M. J. MacLachlan, *J. Mater. Chem.*, 2007, **17**, 1923.
32 (*a*) H. Tong, L. Wang, X. Jing and F. Wang, *Macromolecules*, 2003, **36**, 2584; (*b*) D. Wang, J. Wang, D. Moses, G. C. Bazan and A. J. Heeger, *Langmuir*, 2001, **17**, 1262; (*c*) X. H. Zhou, J. C. Yan and J. Pei, *Macromolecules*, 2004, **37**, 7078.
33 (*a*) M. C. Daniel and D. Astruc, *Chem. Rev.*, 2004, **104**, 293; (*b*) C. Burda, X. Chen, R. Narayanan and M. A. El-Sayed, *Chem. Rev.*, 2005, **105**, 1025.
34 B. C. Sih and M. O. Wolf, *Chem. Commun.*, 2005, 3375.
35 M. K. Corbierre, N. S. Cameron, M. Sutton, S. G. J. Mochrie, L. B. Lurio, A. Rühm and R. B. Lennox, *J. Am. Chem. Soc.*, 2001, **123**, 10411.
36 A. K. Boal, F. Ilhan, J. E. DeRouchey, T. Thurn-Albrecht, T. P. Russell and V. M. Rotello, *Nature*, 2000, **404**, 746.
37 R. Shenhar and V. M. Rotello, *Acc. Chem. Res.*, 2003, **36**, 549.
38 A. K. Boal, T. H. Galow, F. Ilhan and V. M. Rotello, *Adv. Funct. Mater.*, 2001, **11**, 461.
39 O. Uzun, B. L. Frankamp, A. Sanyal and V. M. Rotello, *Chem. Mater.*, 2006, **18**, 5404.
40 J. B. Carroll, B. L. Frankamp and V. M. Rotello, *Chem. Commun.*, 2002, 1892.
41 G. Cooke, J. F. Garety, S. G. Hewage, G. Rabani, V. M. Rotello and P. Woisel, *Chem. Commun.*, 2006, 4119.
42 J. B. Carroll, B. L. Frankamp, S. Srivastava and V. M. Rotello, *J. Mater. Chem.*, 2004, **14**, 690.
43 B. L. Frankamp, O. Uzun, F. Ilhan, A. K. Boal and V. M. Rotello, *J. Am. Chem. Soc.*, 2002, **124**, 892.
44 T. Huang and R. W. Murray, *Langmuir*, 2002, **18**, 7077.
45 P. P. H. Cheng, D. Silvester, G. Wang, G. Kalyuzhny, A. Douglas and R. W. Murray, *J. Phys. Chem. B*, 2006, **110**, 4637.
46 B. I. Ipe, K. G. Thomas, S. Barazzouk, S. Hotchandani and P. V. Kamat, *J. Phys. Chem. B*, 2002, **106**, 18.
47 (*a*) X. He, H. Liu, Y. Li, S. Wang, Y. Li, N. Wang, J. Xiao, X. Xu and D. Zhu, *Adv. Mater.*, 2005, **17**, 2811; (*b*) X. H. Zhou, J. C. Yan and J. Pei, *Macromolecules*, 2004, **37**, 7078; (*c*) X. He, Z. Zhong, Y. Guo, J. Lv, J. Xu, M. Zhu, Y. Li, H. Liu, S. Wang, Y. Zhu and D. Zhu, *Langmuir*, 2007, **23**, 8815.
48 (*a*) H. C. Lin, H. Y. Sheu, C. L. Chang and C. Tsai, *J. Mater. Chem.*, 2001, **11**, 2958; (*b*) H. C. Lin, Y. S. Lin, Y. S. Lin, Y. T. Chen, I. Chao and T. W. Li, *Macromolecules*, 1998, **31**, 7298.
49 (*a*) H. C. Lin, C. M. Tsai, G. H. Huang and Y. T. Tao, *Macromolecules*, 2006, **39**, 557; (*b*) C. W. Wu and H. C. Lin, *Macromolecules*, 2006, **39**, 7985.
50 M. Portugall, H. Ringsdorf and R. Zentel, *Makromol. Chem.*, 1982, **183**, 2311.
51 G. G. Guilbault, *Practical Fluorescence*, Marcel Dekker Inc., New York, 1990.
52 (*a*) S. E. Odinokov, A. A. Mashkovshky, V. P. Glazunov, A. V. Iogansen and B. V. Rassadin, *Spectrochim. Acta*, 1976, **32A**, 1355; (*b*) J. Y. Lee, P. C. Painter and M. M. Coleman, *Macromolecules*, 1988, **21**, 954.
53 B. G. Tehan, E. J. Lloyd, M. G. Wong, W. R. Pitt, J. G. Montana, D. T. Manallack and E. Gancia, *Quant. Struct.-Act. Relat.*, 2002, **21**, 457.
54 E. L. Cabarcos and S. A. Carter, *Macromolecules*, 2005, **38**, 4409.